Scalable Synthesis of the Transparent Conductive Oxide SrVO₃

Lishai Shoham, Maria Baskin, Myung-Geun Han, Yimei Zhu and Lior Kornblum*

L. Shoham, Dr. M. Baskin, Prof. L. Kornblum

Andrew & Erna Viterbi Department of Electrical Engineering, Technion – Israel Institute of Technology, Haifa 32000-03, Israel

E-mail: liork@ee.technion.ac.il

Myung-Geun Han, Yimei Zhu

Condensed Matter Physics & Materials Science, Brookhaven National Laboratory, Upton, New York 11793, United States

The correlated metal SrVO₃ is an attractive earth-abundant transparent conducting oxide (TCO), a critical component of many optoelectronic and renewable energy devices. A key challenge is to synthesize films with low resistivity, due to the prevalence of defects that cause electron scattering. In addition to the material's promise as a TCO, its interesting correlated-electron physics is often obscured by a high defect concentration, which inhibits its further development into new types of electronic devices. Here, a route to synthesize low-defect SrVO₃ films by scalable, industry-compatible molecular beam epitaxy (MBE) is demonstrated. The resulting films consistently exhibit a residual resistivity ratio in the excess of 10 and room temperature resistivity as low as 32 μΩcm, an indication of their high quality and potential for applications. Analysis of the structural and electronic properties of SrVO₃ films provides insights that are applicable to other conductive oxides, and highlights a route for further improvement in their quality and low temperature performance. MBE is the only growth method that allows atomically-abrupt epitaxial interfaces between oxides and semiconductors such as Si and GaAs. Such interfaces are essential for efficient charge transport that is at the heart the performance of most optoelectronic and solar devices.

Transparent conductive oxides (TCOs) constitute an important part of many optoelectronic and renewable energy systems. To maximize device efficiencies, the TCO needs to collect charges from the optically active element, which is commonly a semiconductor such as Si and GaAs, and transport them with minimal electrical and optical losses. TCOs therefore require low resistivity and high optical transmission. It is also desirable to obtain these properties while using earth-abundant materials, which is a bottleneck for the current common TCO, indium tin oxide (ITO), due to the scarcity of indium. .

Recently, the correlated metal strontium vanadate ($SrVO_3$, SVO) has been gaining considerable attention for its potential as a TCO.[1–3] This material is superior in conductivity to ITO,[1] and it is composed of abundant elements. In addition to its potential as a TCO, SVO constitutes the metallic endmember of several Mott-insulating system such as $La_{1-x}Sr_xVO_3$.[4–6] These systems attract interest both for their fundamental physics[7] and their potential for novel types of Mott-electronics.[8,9] It is therefore highly desirable to synthesize high quality films of this material, in order to unlock its full potential as TCO and to allow access to its interesting fundamental physics without the masking of high defect concentrations.

To date, the highest quality SVO films have been demonstrated via hybrid molecular beam epitaxy (hMBE), where vanadium is supplied by a metal-organic precursor and strontium by a conventional thermal source.[10–12] In hMBE, by carefully calibrating the growth parameters, a *self-limiting growth window* can be obtained,[11,13–17] which provides the ultimate route for precise stoichiometry.[18]

The lattice constant of epitaxial oxides provides a sensitive probe of their order and stoichiometry.[19] In addition, for many conductive oxides the residual resistivity ratio, *RRR*, is the most accurate probe,[20] since its sensitivity to defects far exceeds that of most structural and chemical analyses. RRR is the ratio between the room temperature and low temperature (2~5 K) resistivity. Based on Matthiessen's rule, RRR gauges the relative scattering by lattice defects versus the phonon scattering, and high values attest to the quality of the crystal structure and accuracy of the

stoichiometry. The hMBE examples above have consistently reported RRR values exceeding 200, demonstrating the unrivalled accuracy of properly-calibrated hMBE. Recently, significant efforts have been applied to understand and optimize the pulsed laser deposition (PLD) and growth kinetics of SVO,[21] with a record RRR value of 11.5 (Ref. [3]).

While hMBE and PLD can be used to grow epitaxial oxides on conventional semiconductors,[22–25] an insulating interfacial layer forms at the contact with the semiconductor, preventing efficient charge collection from the substrate. Conventional molecular beam epitaxy (MBE) is the only method to date to allow atomically-abrupt epitaxial interfaces between conducting oxides and conventional semiconductors such as Si and GaAs.[26] Such abrupt interfaces are crucial for efficient transport of charge across the interface.[27–29] Furthermore, MBE is a scalable method that is being used in the industry for decades. These advancements have recently been put to use in renewable energy applications revolving around solar water splitting.[29–31] The ability of MBE to produce high quality SVO constitutes a critical milestone towards its eventual integration as a TCO directly on conventional semiconductors. We address this challenge in this work and report high quality MBE-grown SVO, we describe the growth in detail and study the crystal and electronic structures. Our results chart a course for obtaining highly conductive low-defect SVO films, that could be used as *integrated* TCOs and for novel types of electronic devices.

We grow nominally 75 unit cells thick (~29 nm) epitaxial SVO films on (001) $(LaAlO_3)_{0.3}(Sr_2AlTaO_3)_{0.7}$ (LSAT) substrates using oxide MBE at a background molecular oxygen pressure of ~5×10^{-7} Torr and substrate temperatures of 900 and 1000 °C (see Supporting Information for the full details). In these growth schemes, the most crucial component for obtaining high quality films is the percise control over the cationic stoichiometry,[19] ensuring a 1:1 Sr:V ratio. For this end, a quartz crystal microbalance (QCM) is inserted below the sample position before each growth, and the Sr and V fluxes are calibrated separately for dozens of minutes. Since the QCM is positioned slightly below the substrate, the actual atomic flux on the substrate is smaller, and it is accounted for by a

geometric tooling factor. Our results show that the actual tooling factor varies between Sr and V. This could be the result of different sticking coefficients[32], and geometrical offsets between the crucible lip height and filling levels among different source types.

A typical reflectance high-energy electron diffraction (RHEED) pattern acquired from an SVO film surface after growth (Figure S1) shows streaky features with low background signal, indicative of the high degree of crystallinity of the surface. Deviations from the ideal 1:1 cation ratios increase the lattice parameter due to disorder, providing a sensitive probe to the crystalline quality.[19] XRD patterns of the (002) Bragg peak region (Figure 1a) exhibit the typical variation of the lattice spacing with stoichiometry,[11] with a dip in the out-of-plane lattice parameter at a Sr:V QCM reading of 1.0 for films grown at 900°C. A second series grown at 1000°C exhibited essentially the same XRD data for Sr:V QCM readings of 1.0, 1.05 and 1.1 (Figure 1a,b). The lowest out-of-plane lattice parameter we observe is 3.818±0.001 Å, which is slightly lower than values reported by Moyer et al.[10] Surprisingly, the dip in the lattice parameter is not centered around the 1:1 Sr:V QCM reading, rather it is slightly shifted to the higher values (Figure 1b). This observation will be revisited when discussing the electronic properties.

Extending the range of the XRD up to the (003) reflections rules out the presence of any discernable amounts of foreign phases for all the compositions studied here (Figure S2). A reciprocal space map (RSM) around the (013) peak (Figure 1c) indicates that the films are coherently strained to the substrate. Twinning was observed in the RSM for some of the substrates, which remarkably still hosted some of the highest RRR values reported here. The intrinsic lattice parameter of the films was calculated to be 3.840 Å, following the analysis of Moyer[10] and Brahlek[11] et al. Therefore, the coherent SVO films experience 0.7% of tensile strain. Cross-sectional scanning transmission electron microscopy (STEM) image, acquired in high-angle annular dark-field (HAADF) mode, exhibits atomically-abrupt SVO/LSAT interface with no observable defects (Figure 1d). This observation is

consistent throughout the several µm-long focused ion beam (FIB) prepared cross-section sample (Figure S3).
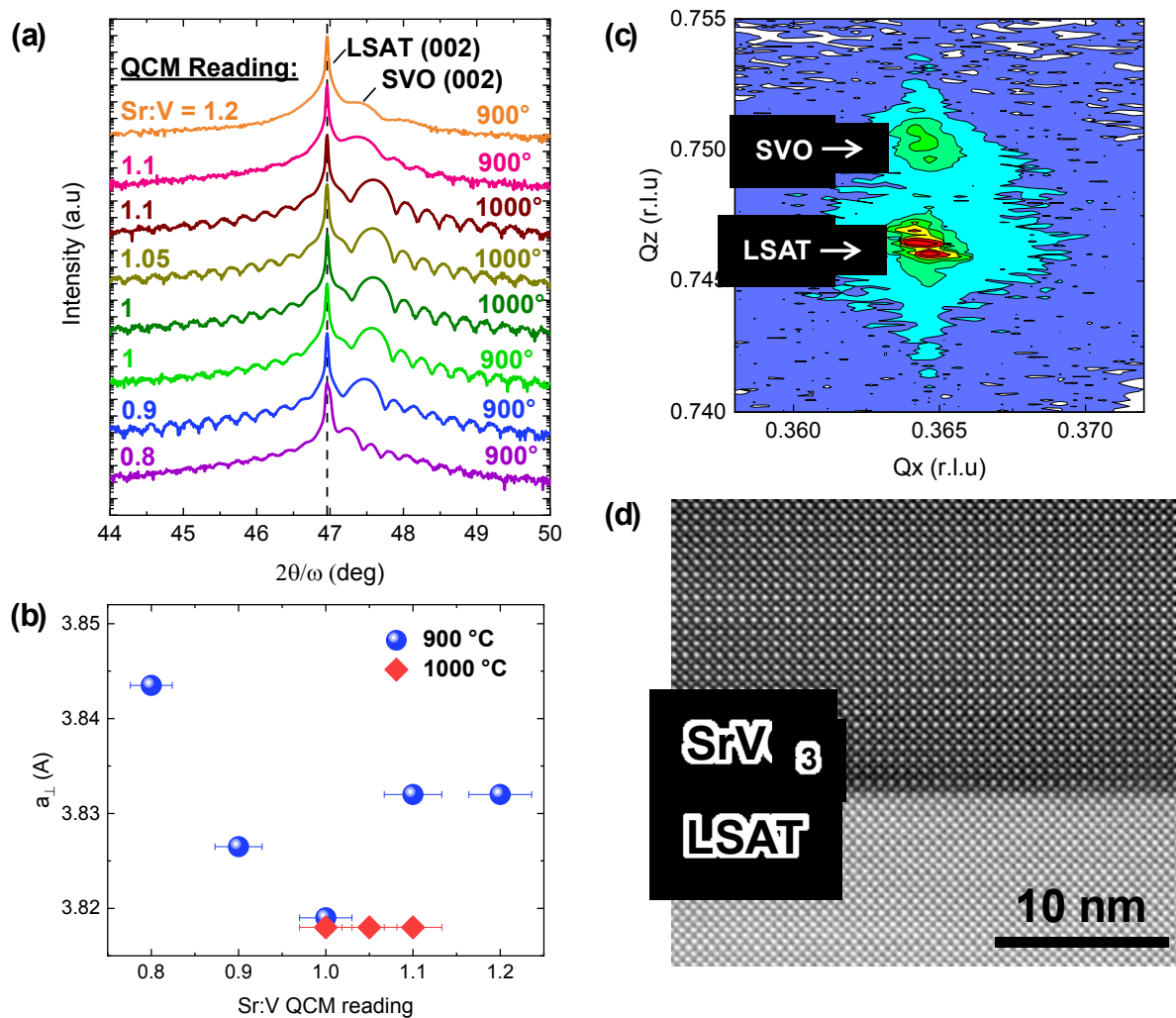
Figure 1. Structural properties of epitaxial SVO films. (a) X-ray diffraction patterns around the (002) Bragg reflection of SVO films grown on LSAT. Varying QCM Sr:V reading ratios are presented grown at 900 and 1000 °C. (b) The relation between the QCM Sr:V reading and the out-of-plane lattice parameter. (c) Reciprocal space map of the sample with Sr:V reading ratio of 1.1, around the (013) reflection, showing a fully strained SVO film on the LSAT substrate. (d) Cross sectional HAADF STEM micrograph of SVO/LSAT taken along the [010] direction of the sample with Sr:V reading ratio of 1.1 (same as panel c).

While the dip in the lattice parameter (Figure 1b) is a sensitive probe for the quality of the films, the most sensitive probe is the temperature dependence of their conductivity, as can be quantified through the RRR. All the films exhibit metallic behavior down to 2 K, and followed the T^2 Fermi liquid behavior for most of the temperature range (Figure 2a). Small deviations from the T^2 behavior at low temperatures are attributed to defect scattering.
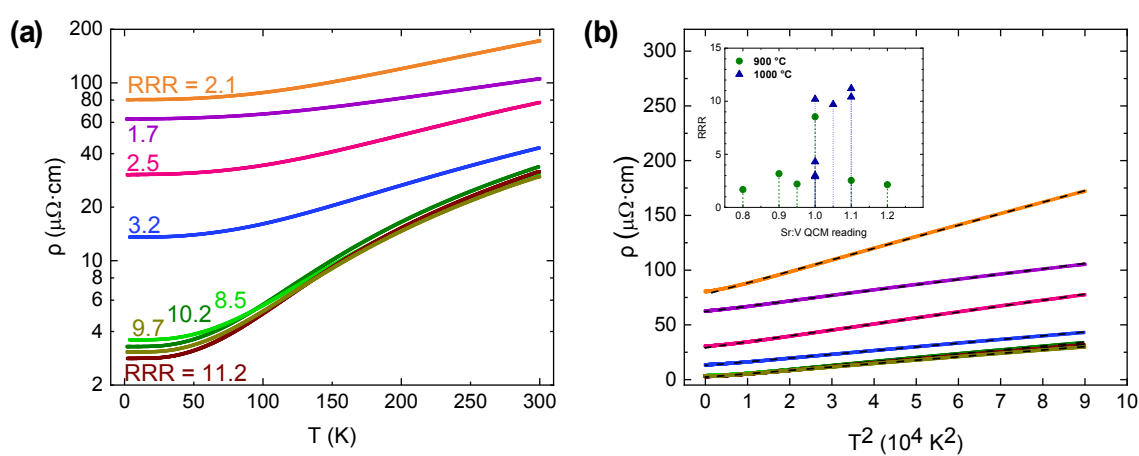
Figure 2. Electronic properties of epitaxial SVO films. (a) ρ-T behavior illustrating the overall low resistivity and high RRR values of the stoichiometric films (see Table 1 for the records). (b) Fermi liquid T^2 dependence of all curves, with a small positive deviation at the lowest temperatures. Inset shows a summary of the RRR values versus the growth conditions. The curves are color-coded consistently with Figure 1.

The dramatic role of the stoichiometry is evident by the large variations of the RRR values, as shown in the inset of Figure 2b. For the most stoichiometric films, an RRR value of 11.2 is observed, with a room temperature resistivity of 32 µΩcm. Hall measurements yield room temperature mobility of 8.2 $cm^2V^{-1}s^{-1}$ and a carrier density of 2.4×10^{22} cm^{-3}. The Hall resistance versus the magnetic field (R_{xy}-B) behavior remains linear up to ±14 T at low temperatures (Figure S4). The room temperature mobility and carrier density values are similar to the best results obtained with PLD,[3] and hMBE[11] (Table 1). The highest RRR values are obtained for Sr:V QCM reading ranging between 1.0 to 1.1 (1000 °C), reproducing a similar trend in the XRD data (Figure 1b). While this behavior (Figure 2b, inset) resembles the growth window in hMBE,[11,14] here no self-limiting growth occurs. Instead, we interpret this behavior as the uncertainty range in the QCM calibration (see Experimental, Supplementary Information), which under the present conditions limits the RRR. Nonetheless, the observed RRR and ρ_{300K} values are among the best reported to date, implying that the effect of this uncertainty is small. These results highlight the advantage of the self-limiting growth afforded by hMBE, which can push the films from almost-stoichiometric to exactly stoichiometric, thus mitigating the uncertainties of flux calibration by QCM or other methods. The removal of this small amount of residual non-stoichiometry defects has significant effect on the low temperature resistivity and thus produces exceptional RRR values. Nonetheless, we note that for room temperature applications (and down to ~100 K and below), the electronic properties of the MBE films are nearly identical to their hMBE counterparts, whereas the RRR difference is mostly manifested in the lowest temperature regime.

Table 1. Transport properties of the most conductive layer, compared to the record parameters obtained by other growth methods: RRR, resistivity, mobility and carrier density. Values refer to $SrVO_3$ grown on LSAT substrates, unless mentioned otherwise.

Growth method	RRR	ρ(300K) $\mu\Omega\cdot cm$	μ(300K) $cm^2V^{-1}s^{-1}$	Carrier density $\times 10^{22}\ cm^{-3}$
MBE, this work	11.2	32	8.2	2.4
hMBE (Refs. [1,10])	>200	30	~9[a]	
PLD (Ref. [3])	11.5	38	~7[a]	~2.6
PLD (NdGaO$_3$ substrates, Ref. [3])	7.5	31	8.3	2.4

[a] values estimated graphically

The Fermi liquid character of the film is manifested by the quadratic temperature dependence of the resistivity (Figure 2). All samples obey the $\rho(T) = \rho_0 + AT^2$ behavior where ρ_0 is the residual resistivity, caused by impurity scattering, and A is the strength of the electron-electron interactions. Fits were done at a temperature range of 50-300 K to avoid the influence of the small positive deviation from the Fermi liquid behavior at very low temperatures. The fits to the ρ-T data (Figure 2b) yielded $A = 3.35 \times 10^{-10}$ $\Omega cm \cdot K^{-2}$ for the highest RRR film, which are of a similar magnitude to previous reports on SVO films[33,34] and bulk samples.[35] The RRR values and Fermi liquid behavior verify the high structural quality of the SVO films, highlighting their potential as effective TCOs. Additionally, this high film quality is important for further studies into their fundamental properties, and may imply their potential as an endmember of Mott-related electronic materials and devices.

The relation between the out-of-plane lattice parameter and the RRR is presented in Figure 3. For the films reported here, when the out-of-plane lattice parameter is under 3.821 Å, the electronic quality (RRR) is significantly improved. While the RRR of the hMBE growth is out of scale, the different growths done by PLD and pulsed electron deposition (PED) agree with our trend. Above ~3.83 Å the RRR seems to have little dependence of the structural properties, which may indicate a saturation of the effect of defect on the scattering. Alternatively, this may imply that the excess cations precipitate to form additional phases, which are disperse enough not to affect electron transport. Precipitates of foreign phases have been observed and analyzed by others in off-stoichiometric films.[12,36] While we were unable to observe such defects in our off-stoichiometric films, in such proximity to 1:1 stoichiometry they might have a low volume fraction below the detection of XRD.
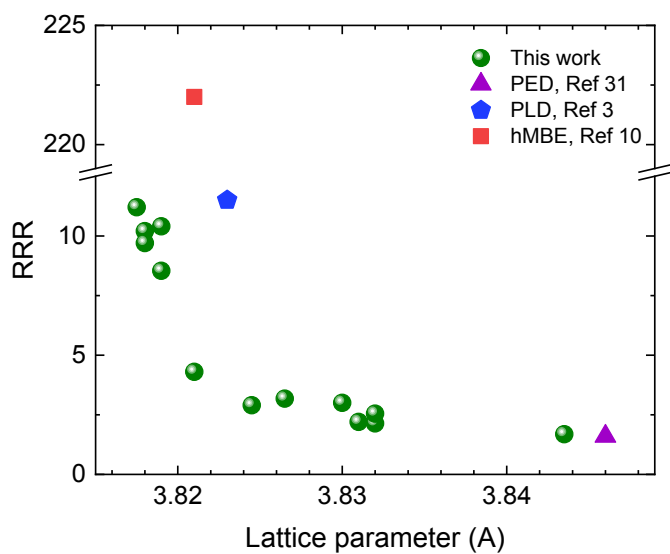
Figure 3. Examination of the out-of-plane lattice parameter of SVO grown on LSAT substrates as a probe for the quality of SVO films. Below a value of 3.821 A, changes of a ~0.2 pm scale have considerable effect on the RRR. The present results are compared to the best reports (for growth on LSAT, for consistency) using pulsed electron deposition (PED), pulsed laser deposition (PLD) and hybrid MBE (hMBE).

Our results suggest further room for increasing RRR with additional control over stoichiometry. This can be achieved by improvement of the QCM operation and the interpretation of its data. While further improvement of the RRR is quite possible, for practical applications such as TCOs, the room temperature resistivity is the key performance metric. In this context, we see that all the high quality films (RRR>8 Figure 2a) have nearly identical room temperature resistivity, comparable to films with RRR>200 (Ref. [10]). The contribution of defect scattering in these high-quality films is therefore already negligible in practical scenarios for TCOs, despite the further improvements that are possible with their RRR.

To fully realize the potential of MBE-grown SVO films, integration on conventional semiconductors[26] is an attractive continuation of this work. The next steps would require finding an appropriate template layer, and addressing band alignment and interfacial charge transfer.[37] We note the high lattice match of SVO to Si (001) of ~ 0.5% (for 45° in-plane rotation). A key challenge would be to circumvent the formation of an insulating interfacial layer, by adapting of the growth conditions for this task. Some degradation in the electronic properties of the oxide is possible due to these limits.[38] However, unlike oxides of the late transition metals, SVO does not require high oxygen pressures or activities; this makes the circumvention of an interface layer far more feasible, in comparison to the silicon integration of other conductive oxides such as ruthenates[39] and manganites.[40]

In conclusion, high quality $SrVO_3$ thin films were epitaxially grown on LSAT substrates using oxide MBE. It is shown that absolute readings of QCM values may result in imperfect cation stoichiometry and a series of varying cation ratios was needed to obtain the highest quality films. After obtaining percise stoichiometry, RRR values of 11.2 and room temperature resistivity of 32 $\mu\Omega$cm are

demonstrated. Furthermore, the high quality of the films is instrumental in the study of the fundamental physics of this correlated metal, without the obstruction of defects. While further optimization of the RRR value are possible, we note that the application-important room temperature resistivity is negligibly affected by the low residual defect resistivity, highlighting the maturity of this approach towards integration with conventional semiconductors. These results pave the way towards leveraging MBE for the growth of high quality transparent conducting electrodes directly on semiconductors.

Supporting Information

The full experimental details, a RHEED image, wide-range XRD scans and Hall measurements are available in the Supporting Information. Supporting Information is available from the Wiley Online Library.

Acknowledgements

Received: ((will   be   filled   in   by   the   editorial   staff))
Revised: ((will   be   filled   in   by   the   editorial   staff))
Published online: ((will be filled in by the editorial staff))

References

[1]   L. Zhang, Y. Zhou, L. Guo, W. Zhao, A. Barnes, H.-T. Zhang, C. Eaton, Y. Zheng, M. Brahlek, H. F. Haneef, N. J. Podraza, M. H. W. Chan, V. Gopalan, K. M. Rabe, R. Engel-Herbert, *Nat Mater* **2015**, *15*, 204.

[2]   K. R. Poeppelmeier, J. M. Rondinelli, *Nat. Mater.* **2015**, *15*, 132.

[3]   M. Mirjolet, F. Sánchez, J. Fontcuberta, *Adv. Funct. Mater.* **2019**, *29*, 1808432.

[4]   P. Dougier, P. Hagenmuller, *J. Solid State Chem.* **1975**, *15*, 158.

[5]   S. Miyasaka, T. Okuda, Y. Tokura, *Phys. Rev. Lett.* **2000**, *85*, 5388.

[6]   M. Uchida, K. Oishi, M. Matsuo, W. Koshibae, Y. Onose, M. Mori, J. Fujioka, S. Miyasaka, S. Maekawa, Y. Tokura, *Phys. Rev. B* **2011**, *83*, 165127.

[7]   M. Imada, A. Fujimori, Y. Tokura, *Rev. Mod. Phys.* **1998**, *70*, 1039.

[8]   I. H. Inoue, M. J. Rozenberg, *Adv. Funct. Mater.* **2008**, *18*, 2289.

[9]   J. Son, S. Rajan, S. Stemmer, S. James Allen, *J. Appl. Phys.* **2011**, *110*, 84503.

[10]   J. A. Moyer, C. Eaton, R. Engel-Herbert, *Adv. Mater.* **2013**, *25*, 3578.

[11]   M. Brahlek, L. Zhang, C. Eaton, H.-T. Zhang, R. Engel-Herbert, *Appl. Phys. Lett.* **2015**, *107*, 143108.

[12]   C. Eaton, J. A. Moyer, H. M. Alipour, E. D. Grimley, M. Brahlek, J. M. LeBeau, R. Engel-Herbert, *J. Vac. Sci. Technol. A* **2015**, *33*, 061504.

[13]   H.-T. Zhang, L. R. Dedon, L. W. Martin, R. Engel-Herbert, *Appl. Phys. Lett.* **2015**, *106*, 233102.

[14]   M. Brahlek, L. Zhang, H.-T. Zhang, J. Lapano, L. R. Dedon, L. W. Martin, R. Engel-Herbert, *Appl. Phys. Lett.* **2016**, *109*, 101903.

[15]   B. Jalan, P. Moetakef, S. Stemmer, *Appl. Phys. Lett.* **2009**, *95*, 032906.

[16]   A. Prakash, P. Xu, X. Wu, G. Haugstad, X. Wang, B. Jalan, *J. Mater. Chem. C* **2017**, *5*, 5730.

[17]   A. Prakash, J. Dewey, H. Yun, J. S. Jeong, K. A. Mkhoyan, B. Jalan, *J. Vac. Sci. Technol. A* **2015**, *33*, 60608.

[18]   M. Brahlek, A. Sen Gupta, J. Lapano, J. Roth, H.-T. Zhang, L. Zhang, R. Haislmaier, R. Engel-Herbert, *Adv. Funct. Mater.* **2018**, *28*, 1702772.

[19]   C. M. Brooks, L. F. Kourkoutis, T. Heeg, J. Schubert, D. A. Muller, D. G. Schlom, *Appl. Phys. Lett.* **2009**, *94*, 162905.

[20] H. P. Nair, Y. Liu, J. P. Ruf, N. J. Schreiber, S.-L. Shang, D. J. Baek, B. H. Goodge, L. F. Kourkoutis, Z.-K. Liu, K. M. Shen, D. G. Schlom, *APL Mater.* **2018**, *6*, 46101.

[21] J. Wang, G. Rijnders, G. Koster, *Appl. Phys. Lett.* **2018**, *113*, 223103.

[22] L. Zhang, R. Engel-Herbert, *Phys. status solidi – Rapid Res. Lett.* **2014**, *8*, 917.

[23] L. Zhang, Y. Wang, R. Engel-Herbert, *J. Appl. Phys.* **2016**, *119*, 45301.

[24] L. Zhang, Y. Yuan, J. Lapano, M. Brahlek, S. Lei, B. Kabius, V. Gopalan, R. Engel-Herbert, *ACS Nano* **2018**, *12*, 1306.

[25] D. Diaz-Fernandez, M. Spreitzer, T. Parkelj, D. Suvorov, *Appl. Surf. Sci.* **2018**, *455*, 227.

[26] D. P. Kumah, J. H. Ngai, L. Kornblum, *Adv. Funct. Mater.* **2019**, 1901597.

[27] J. H. Ngai, D. P. Kumah, C. H. Ahn, F. J. Walker, *Appl. Phys. Lett.* **2014**, *104*, 062905.

[28] L. Kornblum, M. D. Morales-Acosta, E. N. Jin, C. H. Ahn, F. J. Walker, *Adv. Mater. Interfaces* **2015**, *2*, 201500193.

[29] L. Kornblum, D. P. Fenning, J. Faucher, J. Hwang, A. Boni, M. G. Han, M. D. Morales-Acosta, Y. Zhu, E. I. Altman, M. L. Lee, C. H. Ahn, F. J. Walker, Y. Shao-Horn, *Energy Environ. Sci.* **2017**, *10*, 377.

[30] L. Ji, M. D. McDaniel, S. Wang, A. B. Posadas, X. Li, H. Huang, J. C. Lee, A. A. Demkov, A. J. Bard, J. G. Ekerdt, E. T. Yu, *Nat Nano* **2015**, *10*, 84.

[31] K. A. Stoerzinger, Y. Du, S. R. Spurgeon, L. Wang, D. Kepaptsoglou, Q. M. Ramasse, E. J. Crumlin, S. A. Chambers, *MRS Commun.* **2018**, *8*, 446.

[32] J. H. Haeni, C. D. Theis, D. G. Schlom, *J. Electroceramics* **2000**, *4*, 385.

[33] M. Gu, S. A. Wolf, J. Lu, *Adv. Mater. Interfaces* **2014**, *1*, 1300126.

[34] B. Bérini, V. Demange, M. Bouttemy, E. Popova, N. Keller, Y. Dumont, A. Fouchet, *Adv. Mater. Interfaces* **2016**, *3*, 1600274.

[35] P. Dougier, J. C. C. Fan, J. B. Goodenough, *J. Solid State Chem.* **1975**, *14*, 247.

[36] Y. Bourlier, M. Frégnaux, B. Bérini, A. Fouchet, Y. Dumont, D. Aureau, *ChemNanoMat* **2019**, *5*, 674.

[37] E. N. Jin, A. Kakekhani, S. Ismail-Beigi, C. H. Ahn, F. J. Walker, *Phys. Rev. Mater.* **2018**, *2*, 115001.

[38] L. Kornblum, J. Faucher, M. D. Morales-Acosta, M. L. Lee, C. H. Ahn, F. J. Walker, *J. Appl. Phys.* **2018**, *123*, 25302.

[39] Z. Wang, H. P. Nair, G. C. Correa, J. Jeong, K. Lee, E. S. Kim, A. S. H., C. S. Lee, H. J. Lim, D. A. Muller, D. G. Schlom, *APL Mater.* **2018**, *6*, 86101.

[40] C. Adamo, L. Méchin, T. Heeg, M. Katz, S. Mercone, B. Guillet, S. Wu, J.-M. Routoure, J. Schubert, W. Zander, R. Misra, P. Schiffer, X. Q. Pan, D. G. Schlom, *APL Mater.* **2015**, *3*, 062504.

Author Manuscript

SrVO$_3$ is a correlated oxide with metallic behavior and optical transparency in the visible, making it an attractive, earth-abundant transparent conductive oxide. We report here the first conventional oxide molecular beam epitaxy of high quality SrVO$_3$ films. This scalable technique provides the stepping stone towards ultimately integrating SrVO$_3$ directly on conventional semiconductors, with numerous prospects of optoelectronic and solar applications.

Keyword transparent conductive oxides, correlated metals, strontium vanadates, epitaxial oxides, functional oxides

Lishai Shoham, Maria Baskin, Myung-Geun Han, Yimei Zhu and Lior Kornblum*

Scalable Synthesis of the Transparent Conductive Oxide SrVO$_3$

ToC figure